

## New observations of martian southern mid-latitude recurring slope lineae (RSL) imply formation by freshwater subsurface flows



David E. Stillman<sup>a,\*</sup>, Timothy I. Michaels<sup>b</sup>, Robert E. Grimm<sup>a</sup>, Keith P. Harrison<sup>a</sup>

<sup>a</sup> Southwest Research Institute, 1050 Walnut St. #300, Boulder, CO 80403, United States

<sup>b</sup> Carl Sagan Center, SETI Institute, 189 Bernardo Ave. Suite 100, Mountain View, CA 94043, United States

### ARTICLE INFO

#### Article history:

Received 6 May 2013

Revised 7 January 2014

Accepted 19 January 2014

Available online 1 February 2014

#### Keywords:

Mars, surface

Geological processes

Ices

Mars, climate

### ABSTRACT

Southern mid-latitude (SML) recurring slope lineae (RSL) are narrow (0.5–5 m) dark albedo features that emanate from bedrock and incrementally lengthen down steep slopes that preferentially face the equator. We observe that SML RSL begin lengthening prior to southern summer at a solar longitude ( $L_s$ ) of  $245^\circ \pm 11^\circ$  when Mars Global Surveyor Thermal Emission Spectrometer (TES)-derived near-maximum surface temperatures are  $296 \pm 5$  K and Mars Reconnaissance Orbiter Mars Climate Sounder (MCS) – and Mars Odyssey Thermal Emission Imaging System (THEMIS)-derived mid-afternoon surface temperatures are  $>273$  K. SML RSL continue to lengthen for  $104 \pm 38$  sols with an average near-maximum surface temperature of  $298 \pm 5$  K. The SML RSL then stop lengthening at  $L_s = 314^\circ \pm 12^\circ$  when mid-afternoon surface temperatures drop below 273 K. They remain dark for another  $116 \pm 41$  sols (until  $L_s = 16^\circ \pm 14^\circ$ ) as surface temperatures continue to fall. Although the RSL recharge mechanism remains unknown, our observation that the vast majority of RSL lengthen only when mid-afternoon surface temperatures are  $>273$  K supports the hypothesis that they are formed by shallow subsurface liquid water flows without significant freezing-point depression. The number and length of RSL at multiple sites increased dramatically following the Mars Year 28 globe-encircling dust storm. We interpret this increase to be due to warmer subsurface temperatures created by a dust-laden greenhouse effect that may be unique to the southern mid-latitudes near  $L_s = 270^\circ$ . Therefore SML RSL flow is quite sensitive to ground temperature and may only occur under favorable orbital parameters when mean insolation during the RSL lengthening season is above that of the current southern mid-latitude mean insolation value. This value is currently at a peak that has not been attained for the last  $\sim 100$  ka. Meanwhile, the RSL-poor northern mid-latitude mean insolation is near a minimum and has a value 27% lower than the southern value. If SML RSL are indeed formed by shallow subsurface freshwater flows, then they may be some of the best locations on Mars to explore for extant life.

© 2014 Elsevier Inc. All rights reserved.

### 1. Introduction

Recurring slope lineae (RSL) are defined as narrow features (0.5–5 m)  $<40\%$  darker than their surroundings, that emanate from warm steep slopes ( $\sim 33\text{--}38^\circ$ ) and incrementally lengthen (McEwen et al., 2011). Evidence of surficial material transport has not yet been detected. RSL continue to be identified in images from the Mars Reconnaissance Orbiter (MRO) High Resolution Imaging Science Experiment (HiRISE, McEwen et al., 2007). RSL are relatively rare with only  $\sim 60$  candidate or confirmed locations, distributed in three geographical regions: a southern mid-latitude band ( $31\text{--}52^\circ\text{S}$ ), an equatorial band ( $18\text{--}4^\circ\text{S}$ ), and four sites in the

northern latitude band ( $10\text{--}37^\circ\text{N}$ ) (McEwen et al., 2011, 2013; Ojha et al., 2013). Mid-latitude RSL are typically found on equator facing slopes. Southern mid-latitude (SML) RSL start slightly before southern solstice and remain dark until slightly after the southern autumnal equinox, when peak observed surface temperatures were reported to be  $\sim 250\text{--}300$  K, (McEwen et al., 2011). The majority of equatorial RSL are found in Valles Marineris and their seasonality is a function of the slope orientation (McEwen et al., 2013).

Four formation hypotheses were suggested by McEwen et al. (2011): wet debris flow, dry dust avalanche or grain flow, brine flow in the shallow subsurface, and briny surface flow. These hypotheses were deemed imperfect, with the wet debris and brine flow hypotheses lacking a sufficient source of water, and debris flows missing a mechanism that can create yearly recurrence at

\* Corresponding author.

E-mail address: [dstillman@boulder.swri.edu](mailto:dstillman@boulder.swri.edu) (D.E. Stillman).

the same location while not altering topography. To further complicate matters, targeted MRO Compact Reconnaissance Imaging Spectrometer for Mars (CRISM) observations ( $\sim 18$  m/pixel) do not conclusively identify an enhancement in water or salt (McEwen et al., 2011). Levy (2012) found that a simple saturated porous flow model was consistent with an RSL hydraulic conductivity corresponding to silty sand to well-sorted sand. Chevrier and Rivera-Valentin (2012) used a thermodynamic and kinetic model to suggest that RSL are formed via melting of a brine with a freezing point of  $\sim 223$  K within 20 cm of the surface. These conditions yield low evaporation rates that favor persistence of deep subsurface liquid into southern martian autumn ( $L_s = 45^\circ$ ).

This paper outlines a formation mechanism consistent with observations of SML RSL sites. We restrict this investigation to SML RSL because at the time of our analysis this was the most complete data set. We first describe the methodology of our data analysis and then detail our new observations. These observations are then used to postulate a flow mechanism for SML RSL formation, with further discussion regarding the variability induced by the Mars Year 28 globe-encircling dust storm and long-term recurrence frequency. We also compare our flow mechanism to other RSL observational and modeling work, and discuss anomalous observations and the possible astrobiological significance of RSL. We conclude that SML RSL are caused by subsurface shallow liquid water flows. In a companion paper (Grimm et al., in press, hereafter Paper II) we use these results as constraints on numerical models of RSL flow and show that the small water volumes ( $2\text{--}10$  m<sup>3</sup> of H<sub>2</sub>O per m of source headwall for continuous extrusion and  $0.2\text{--}2$  m<sup>3</sup>/m for intermittent flow) required are consistent with the hypothesis of localized fresh meltwater.

## 2. Methodology

We analyzed images and derived surface temperatures at 15 candidate and 17 confirmed (the latter show recurrence and incremental lengthening whereas the former lack repeat HiRISE images to demonstrate recurrence or incremental lengthening) SML RSL locations. High resolution ( $\sim 0.3$  m per pixel) HiRISE images allowed us to observe seasonal albedo variations of the RSL. Images from the  $\sim 6$  m per pixel Context Camera (CTX, Malin et al., 2007) onboard MRO and the  $\sim 100$  m per pixel 2001 Mars Odyssey Thermal Emission Imaging System (THEMIS, Christensen et al., 2004) Day IR Global Mosaic (v 11.5) were used to provide context for the HiRISE imagery. We examined each HiRISE image acquired between December 26, 2006 and September 2, 2013 at candidate and confirmed SML RSL locations. Each image was then analyzed to determine if RSL were visible, and to establish the orientation of slopes with RSL. We also referenced earlier imagery to determine if the RSL had lengthened or faded. For each SML RSL site additional observations were made regarding the geomorphology surrounding the site, drainage pattern, source type (bedrock or regolith), source elevation, and any other unique features of the site. A spreadsheet of our observations can be found in the [supplemental data](#).

To constrain the thermal conditions of SML RSL activity, surface temperatures of RSL locations were extracted from daytime data acquired by Mars Global Surveyor Thermal Emission Spectrometer (TES, Christensen et al., 2001), from nadir measurements taken by MRO Mars Climate Sounder (MCS; McCleese et al., 2007), and from THEMIS brightness temperature retrievals. The TES data do not overlap temporally with HiRISE RSL observations and were acquired from February 1999 to October 2006 at a local true solar time (LTST) of  $\sim 13.3\text{--}14.7$  Mars-hours. TES data have a relatively low spatial resolution of  $\sim 3 \times 6$  km; therefore temperatures on warmer equator-facing steep slopes hosting the RSL are averaged

with cooler surface features. The Planetary Data System TES daytime surface temperatures were calculated by finding the maximum brightness temperature over 100 spectral channels from  $7.4$  to  $12.5$   $\mu\text{m}$  ( $1350\text{--}800$  cm<sup>-1</sup>) and  $20\text{--}33.3$   $\mu\text{m}$  ( $500\text{--}300$  cm<sup>-1</sup>), with the  $7.7$   $\mu\text{m}$  ( $1300$  cm<sup>-1</sup>) band typically having both the maximum value and the least interference from atmospheric effects (Christensen, 2006).

MCS data overlap temporally with HiRISE RSL observations and were acquired over RSL sites from September 25, 2006–January 31, 2013. We used the second recalibrated version of the Derived Data Records (DDRs). These data were collected at a varying LTST of  $14.2\text{--}15.3$  Mars-hours for daytime data at SML RSL sites and have a spatial resolution of  $2\text{--}6$  km (Hayne et al., 2012).

THEMIS data overlap temporally with HiRISE RSL observations and were acquired over RSL sites from February 20, 2002–March 31, 2012. These data were collected at a varying LTST of  $14.4\text{--}17.6$  Mars-hours at SML RSL sites and have a higher spatial resolution ( $\sim 100$  m per pixel) than either TES or MCS. Therefore, multiple pixels were chosen over the areas where RSL occur. This allowed us to compute a minimum, average, and maximum value for each THEMIS image. However,  $\sim 40\%$  of the THEMIS surface temperatures at the RSL locations are clipped. This seems to have occurred because the THEMIS image is overexposed (saturated) in the warmest areas, resulting in broad areas with the same derived temperature. This implies that actual surface temperatures must be greater than the value indicated by THEMIS. THEMIS brightness temperature data products were constructed by mapping the brightness temperature at  $12.57$   $\mu\text{m}$  ( $800$  cm<sup>-1</sup>), assuming an emissivity of 1 and atmospheric opacity of 0 (Christensen, 2003). Furthermore, TES has shown that brightness temperature and thus emissivity peaks near  $\sim 7.7$   $\mu\text{m}$  ( $1300$  cm<sup>-1</sup>) for warmer ground surfaces (e.g., those  $>225$  K; Christensen, 2006). Therefore, these THEMIS temperature values are generally lower limits.

## 3. Observations

### 3.1. RSL duration

McEwen et al. (2011) categorized SML RSL with and without activity at the then seven confirmed RSL sites over three MY, finding that SML RSL were active from  $L_s = 240^\circ$  to  $20^\circ$ . RSL were considered active if the entire RSL had an albedo that was darker than the background and inactive if all or a portion of the RSL had an albedo that was indistinguishable from background albedo. We categorized each HiRISE image from the 32 candidate and confirmed SML RSL sites over four MY into one of five RSL categories (Figs. 1 and 2). (1) Dark and lengthening RSL, consisting of dark albedo features that incrementally lengthen in subsequent images. (2) Dark and static RSL, consisting of dark albedo features that do not incrementally lengthen in subsequent images. (3) “RSL”, where dark albedo features were detected, but no recent (within  $90^\circ$  of  $L_s$ ) images are available for comparison. (4) Partially faded RSL, where a portion of the relevant albedo features have faded back to the albedo of the surrounding terrain. (5) Completely faded RSL, consisting of known sites that no longer have an albedo contrast (within a few percent) with the surrounding terrain. The range of  $L_s$  values corresponding to each category is given in Table 1. We assume that SML RSL are only active if they are lengthening, yielding an active period of  $L_s = 248 \pm 11^\circ$  to  $314 \pm 12^\circ$  ( $104 \pm 38$  sols), or 136 fewer sols than the McEwen et al. (2011) estimate.

Note that the SML RSL duration values given in Table 1 and Fig. 2 are the time RSL lengthen at a site. Individual RSL typically lengthen over a shorter period of time as lengthening at one individual RSL causes the entire RSL site to be considered active. As more data is gathered each RSL site will likely have its own unique

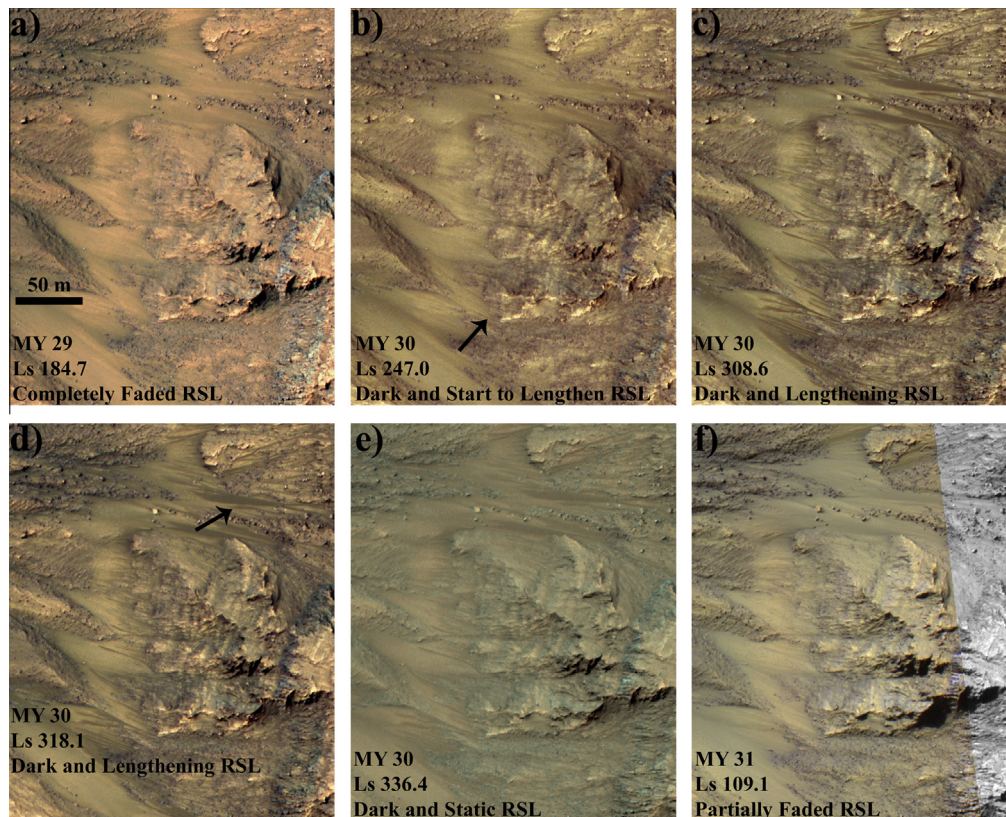


**Fig. 1.** Visual description of RSL categories at Palikir crater (41.6°S, 202.3°E): (a) completely faded RSL, (b) dark RSL but no recent images to determine lengthening, (c, d) dark and lengthening RSL, (e) dark and static RSL, and (f) partially faded RSL. Note that in (e) the RSL albedo has increased from (d), however this is still considered dark because the entire RSL still maintains an albedo that is darker than the background. (b) The most visible RSL is depicted by the arrow, however at higher resolution the scree slope to the east of the arrow is dominated by multiple RSL that merge into the one highlighted by the arrow. This indicates that the RSL started lengthening before  $L_s = 247^\circ$ . There are actually three subsequent images between (b) and (c) that show the incremental movement of RSL. (d) There is only a slight lengthening of a single RSL highlighted by the arrow, although not visible at this scale. This observation, combined with the lack of lengthening in (e) indicates that the RSL stopped lengthening between  $L_s 308.6^\circ$  and  $318.1^\circ$ . (e) RSL are darker than their surroundings, but no longer move. Also note that the dark albedo signature of the RSL has begun to lighten. (f) The dark albedo of many of the RSL has faded to that of the background, while others are still barely visible. Images (a–d) were taken from the animated gif ([http://hirise.lpl.arizona.edu/sim/images/science\\_aug/Newton\\_IRB\\_A.ORTHO-stretch-enh-crop5\\_leg.gif](http://hirise.lpl.arizona.edu/sim/images/science_aug/Newton_IRB_A.ORTHO-stretch-enh-crop5_leg.gif)) released with McEwen et al. (2011). Images for (e) and (f) are not orthorectified and are cropped HiRISE images ESP\_23467\_1380 and ESP\_27146\_1380.

duration based on its thermal properties, latitude, and RSL slope direction. However, even at each SML RSL site there are variations. For example, RSL in Palikir crater (41.6°S, 202.3°E) start from western-facing slopes before northwest-facing slopes. Given that the aliased temporal coverage and spatial resolutions are of a scale similar to that of an individual RSL, we find that when we first detect RSL, their lengths are already  $\sim 10$  m. This indicates that given better temporal coverage, RSL will start earlier than we have observed to date.

We then compared the TES-, MCS-, and THEMIS-derived surface temperatures to SML RSL seasonality (Fig. 3). Using our largest data set (TES-derived), we found no significant deviation in temperature as a function of RSL-site latitude (Fig. S1). Assuming latitude independence, the seasonally aliased data can be combined to create a more complete representation of seasonal surface temperature (Fig. 3). Overall, we found that SML RSL start and stop lengthening when the TES-derived near-maximum early afternoon surface temperatures are  $296 \pm 5$  K and  $289 \pm 9$  K, respectively (Fig. 3a). SML RSL lengthen when near-maximum surface temperatures and MCS-derived mid-afternoon surface temperatures have average values of  $298 \pm 5$  K and  $282 \pm 6$  K, respectively (Fig. 3a and b). THEMIS-derived mid-afternoon average surface temperatures during SML RSL lengthening cannot be used in the same quantitative fashion because so many data are saturated. However, mid-afternoon surface temperatures measured by MCS and THEMIS

show that SML RSL only lengthen when the temperature is greater than the freezing point of pure liquid water on Mars ( $273.16$  K) (Fig. 3b and c).

### 3.2. Post Mars Year 28 dust storm

RSL sites imaged in Mars Year (MY, Clancy et al., 2000) 28 show a significant increase in number of RSL per site (McEwen et al., 2011) and RSL length compared to the subsequent years (Figs. 4 and 5). While RSL typically appear to emanate from bedrock (McEwen et al., 2011), many SML RSL sites in MY 28 appear to also emanate from non-bedrock sources at small divides in the topography (Figs. 5 and 6). MY 28 coincided with extensive southern hemisphere dust storm activity that eventually resulted in a globe-encircling dust pall. Dust opacities measured by the Mars Exploration Rovers show that this pall lasted the majority of the RSL active season from  $L_s \sim 265$  to  $\sim 326^\circ$  (Fig. S2). We agree with the interpretation of McEwen et al. (2011) that the very thin layer of bright dust allows RSL to be detected more easily due to a higher contrast. However, we do not believe that this is the root cause of the increase in RSL density and lengthening. In southwest Asimov Crater, RSL were not detected in MY 30 at the same locations where they have the greatest albedo contrast and where they are the widest in MY 28 (Fig. 4). Similar phenomena are also observed to occur at the central peak of Lohse Crater (Fig. 5). Indeed, some of

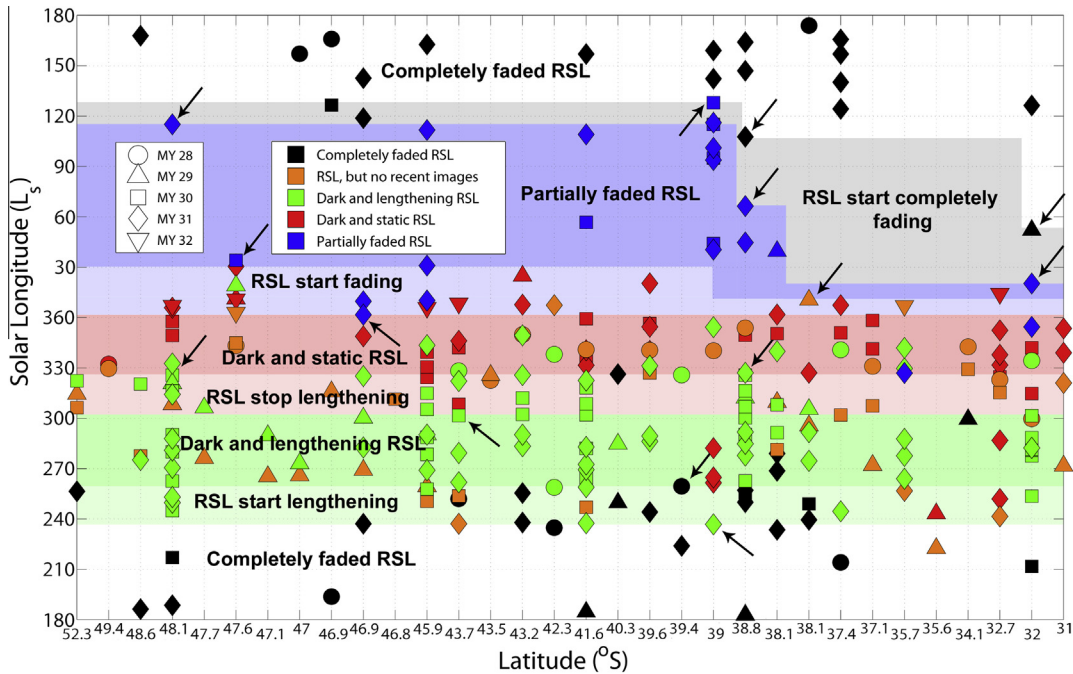


**Fig. 2.** SML RSL seasonality is displayed by plotting  $L_s$  against 32 candidate and confirmed SML RSL sites poleward of  $31^\circ\text{S}$ . Note that the x-axis is not linear, and each labeled latitude value represents an RSL location that corresponds to a candidate or confirmed SML RSL site. The data table for this figure can be found in the spreadsheet in the [supplemental material](#). The arrows point to data symbols that were used to interpret the boundaries. The results of this interpretation are shown in [Table 1](#). The only possible latitude-dependent trend is the transition between the partially faded RSL and completely faded RSL, but more data is needed to be confident about this trend. Outliers are discussed in [Section 5.4](#).

**Table 1**

Duration of SML RSL activity. The latitude-dependent fading equatorward of  $39^\circ\text{S}$  is not given due to lack of data.

RSL Phase	$L_s$ range	Number of sols
Dark and lengthening	$248^\circ \pm 11^\circ$ – $314^\circ \pm 12^\circ$	$104 \pm 38$
Dark and static	$314^\circ \pm 12^\circ$ – $16^\circ \pm 14^\circ$	$116 \pm 41$
Partially faded poleward of $39^\circ\text{S}$	$16^\circ \pm 14^\circ$ – $117.5^\circ \pm 1^\circ$	$220 \pm 32$
Completely faded poleward of $39^\circ\text{S}$	$117.5^\circ \pm 1.4^\circ$ – $248^\circ \pm 11^\circ$	$228 \pm 21$

the darkest RSL albedo locations in southwest Asimov Crater are actually lighter than the surrounding material ([Fig. 4](#)). We suggest in [Section 5.1](#) that the RSL density and length increased in MY 28 due to subsurface warming caused by the dust pall. Unfortunately, surface temperature data from MCS have not been reduced during the dust pall due to the complications of removing atmospheric opacity effects.

### 3.3. RSL slope asymmetries and correlation with gullies

SML RSL occur more frequently on equator- and west-facing slopes than pole- and east-facing slopes ([Fig. 7](#)). RSL can be detected within shadows in HiRISE imagery, so we do not believe that the east–west bias is due to the favorable illumination of west-facing slopes. This is likely due to the fact that the subsolar point is always equatorward of these locations, and the increased downward infrared radiation from the warmer afternoon atmosphere (versus that in the morning) favors west-facing slopes. This further underscores the sensitivity of SML RSL to temperature.

We concur with the suggestion by [McEwen et al. \(2011\)](#) that SML RSL and gullies are likely linked. The majority of sites have RSL in equator-facing fine gullies and channels and a few even possess RSL in pole-facing large alcove-channel-apron gullies ([Fig. 8](#)). RSL are only found in the source zone or alcove of these gullies

([Fig. 9](#)). SML RSL follow the same dendritic drainage pattern as the gullies, with nearly all RSL merging with other RSL ([Fig. 6c](#)). SML RSL likely emanate from the same bedrock source as equator-facing fine gullies and channels ([Fig. 9](#)). However, the need for a bedrock source for pole-facing large alcove-channel-apron gullies is still debated (e.g., [Dundas et al. 2012](#)) (see [Figs. 10 and 11](#)).

### 3.4. RSL type and correlation with volatiles

We categorized the candidate and confirmed SML RSL sites into three types based on regional geomorphology ([Table 2](#), see [supplemental data spreadsheet](#)). No single RSL type dominates, although fresh craters  $<10$  km in diameter (Type Ia or IIa) are the most common RSL host. Type III RSL occur along any steep slope of large craters ( $>10$  km) with bedrock that has a small component facing the equator. We estimate that the 80 km diameter Asimov crater may have RSL activity along  $\sim 150$  km of its steep-sloped rim ([Fig. 12](#)) as RSL are present in every HiRISE image acquired in the appropriate season.

## 4. RSL formation and recharge mechanisms

We used the following observations and interpretations to develop a conceptual model for SML RSL in which RSL are caused by liquid water flowing in the shallow subsurface:

1. The vast majority of SML RSL only lengthen when mid-afternoon surface temperatures are  $>273$  K ([Figs. 2 and 3](#)). This suggests that RSL lengthening is correlated to the freezing point of pure liquid water.
2. Immediately after the MY 28 dust storm, RSL were longer and emanated from more sources including non-bedrock sources ([Figs. 4–6](#)). This suggests that a globe-encircling dust storm can raise subsurface temperatures above typical non-dust-storm year values, producing longer and more abundant RSL.

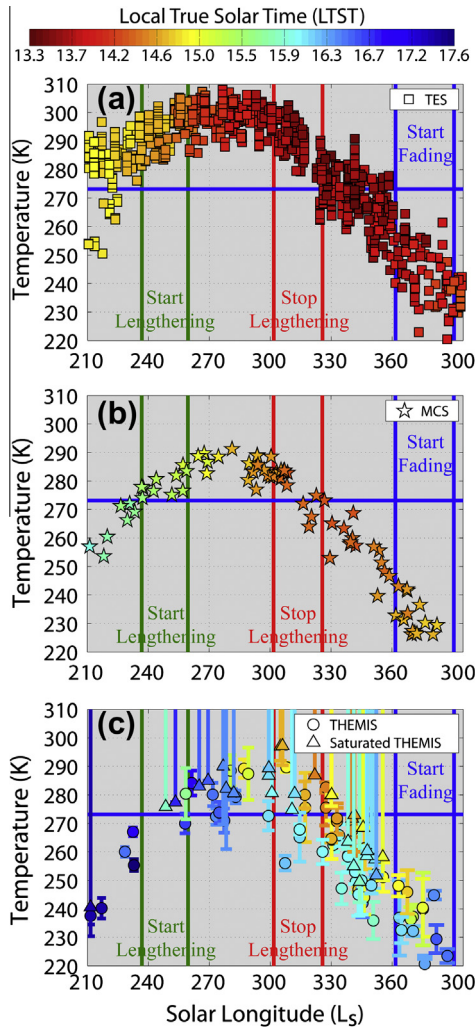


**Fig. 3.** (a) TES-, (b) MCS-, and (c) THEMIS-derived surface temperatures at all RSL sites as a function of  $L_s$  with symbol color indicating LTST. These plots show that afternoon surface temperatures are always greater than the melting point of pure water at 273.16 K (horizontal blue line). After SML RSL stop lengthening, all surface temperatures fall below the freezing point. The error bars on the THEMIS data indicate the minimum and maximum temperature measured at the RSL location. If the minimum and the average (given by the triangle) correspond, this indicates that every pixel at the RSL location was clipped. Clipped THEMIS data are shown with no maximum error bar.

3. RSL typically emanate from bedrock (Figs. 4 and 9). This suggests that RSL emanate from bedrock due to a difference in material properties versus that of regolith.

#### 4.1. Recharge mechanisms

The exact mechanism that provides recharge to the RSL remains poorly understood. At least three possible scenarios exist: annual cold trapping of ice, shallow liquid aquifers (Malin and Edgett, 2000; Mellon and Phillips, 2001), or deliquescence of salts (Gough et al., 2011; McEwen et al., 2013; Wang et al., 2013). Here we discuss the former as it has not previously been discussed. Annual cold trapping of ice could occur within meters of the surface when the high thermal conductivity of the outcropping bedrock cools this layer beneath the average subsurface temperature. This would assume that the “atmosphere” within the subsurface porosity was nearly saturated with water vapor, possibly originally sourced from the latitude dependent mantle (LDM; Kreslavsky and Head, 2000, 2002; Mustard et al., 2001). This cold trapped ice would then

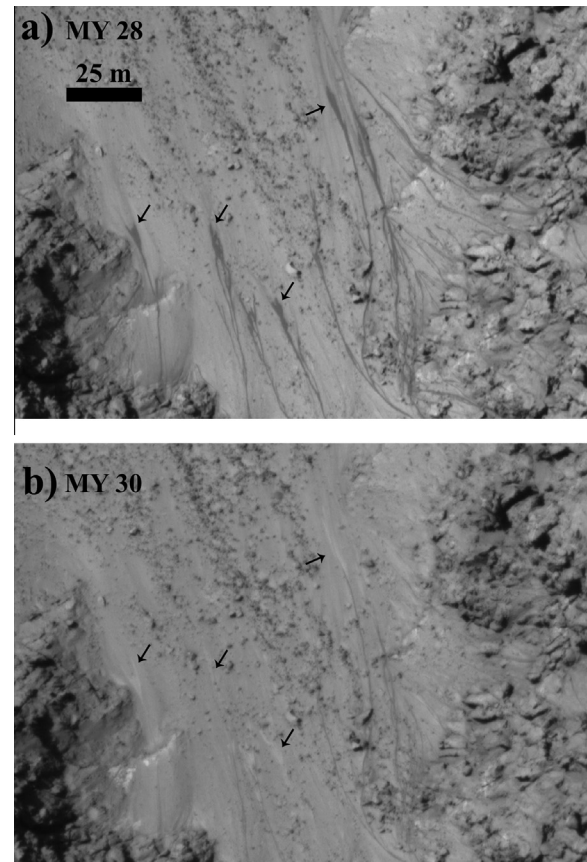


**Fig. 4.** These two images taken almost exactly 2 MY apart in the southwest part of Asimov crater (47.6°S, 4.6°E) demonstrate that RSL in (a) the MY 28 (post dust storm) image are more numerous and longer compared to the (b) MY 30 image. The arrows highlight the differences in the two images. (a) HiRISE image PSP\_006003\_1320 at MY 28  $L_s = 343.3^\circ$ , emission angle  $7.5^\circ$ , phase angle  $56.2^\circ$ . (b) HiRISE image ESP\_023672\_1320 at MY 30  $L_s = 344.9^\circ$ , emission angle  $8.6^\circ$ , phase angle  $56.7^\circ$ .

have to be sublimated once temperatures increased and again cold trapped within a meter of the surface during or before the active SML RSL season in order to melt. Based on the volume estimates of saturated flows in Paper II of 2–10 m<sup>3</sup> of H<sub>2</sub>O per m of headwall, this recharge mechanism would not be able to provide enough water annually. If RSL flows are modeled as intermittent slugs of water that overrun prior parts of the flow with residual water content (like raindrops migrating down a window), then the reduced source volume needed could be from cold trapped water vapor. However, to trap this much ice in one year we estimate that the subsurface atmosphere must be significantly warmer than the annual mean temperature or most of the CO<sub>2</sub> has been evacuated from the subsurface.

#### 4.2. Diurnal melting and water stability

Regardless of the recharge mechanism, our observations confirm that RSL do not flow until the near-maximum and mid-afternoon surface temperatures reach  $\sim 296 \pm 5$  K and  $>273$  K, respectively (Fig. 3). The likely reason that flow does not occur immediately after maximum temperatures reach  $>273$  K is because this heat must diffuse into the subsurface. Using a thermal model that ignores the effects of phase changes, and which uses the thermal properties of a water-saturated regolith (Table 3), we estimate that depths between 5 and 16 cm will experience temperatures above freezing when RSL are flowing (Fig. S5). (Furthermore, a

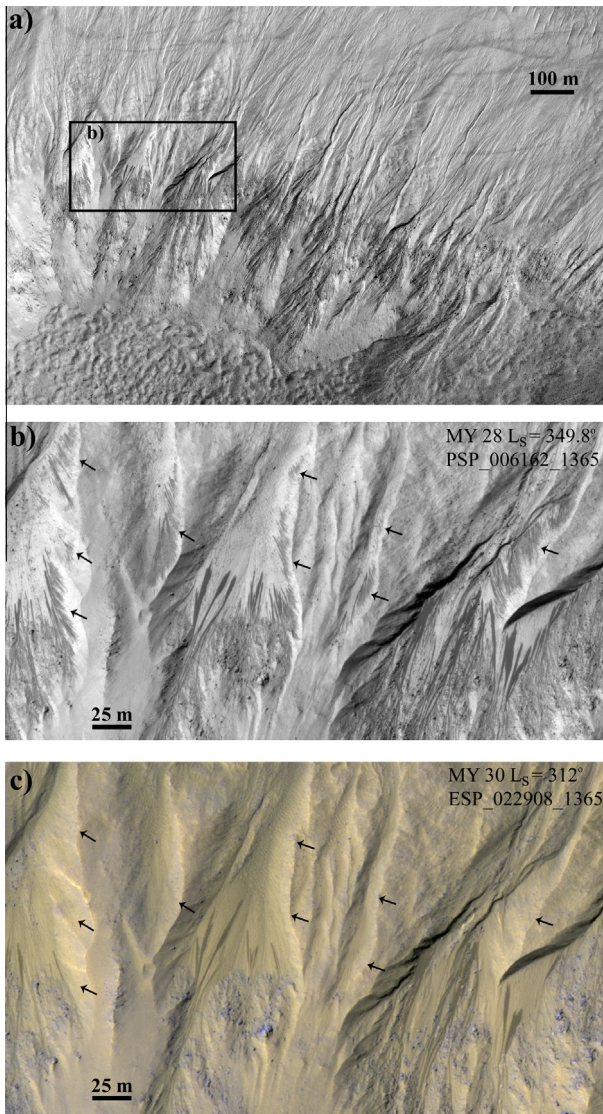


**Fig. 5.** (a) RSL emanate from the steep slopes and lengthen down equator-facing gullies in the central peak of Lohse crater (43.32°S, 343.21°E). (b) Sources (highlighted by arrows) only occur during the MY 28 dust storm and appear to originate out of ridges that do not have outcropping bedrock. (c) MY 30 image of the same area. Arrows highlight the lack of non-outcropping bedrock sources. While these images were not collected at the same  $L_s$ , they are comparable since RSL in both images are presumably at their maximum extent and no new sources would have appeared this late into the season.

more complete thermal model with phase changes is run in Paper II and shows melting to 6 cm at  $L_s$  245°. An atmospheric pressure of  $\geq 6.1$  mbar is also required for stable liquid water. Even though SML RSL occur when martian atmospheric pressure reaches its maximum seasonal value (e.g., Tillman et al., 1993), the elevation of most SML RSL sites indicates local surface pressures below 6.1 mbar. Even at RSL sites with surface pressures above 6.1 mbar, surficial pure liquid water is only metastable for a few kelvins above freezing before it begins to boil. Furthermore, the daytime relative humidity is extremely low (Zent et al., 2010), increasing evaporation of any non-boiling surficial liquid water. Brine solutions increase the stability of water by decreasing the water activity, allowing surface liquid to form at lower atmospheric pressures and boil at higher temperatures.

In sub-eutectic concentrations the evaporation rate is a function of the water activity, with the evaporation rate rarely decreased by

more than 40% compared to that of pure water (e.g., Altheide et al., 2009). To lower the evaporation by a factor of 10 from the pure water evaporation rate at 273.16 K takes a freezing depression of  $\sim 20$  K or a super-eutectic concentration where the evaporation rate is controlled by the formation of salt hydrates (Altheide et al., 2009). However, an overlying low gas-diffusivity regolith can reduce evaporation rates by a factor of 10, regardless of salinity (Chevrier et al., 2007, 2008; Bryson et al., 2008). This decrease in vapor diffusion affords subsurface water greater stability and allows subsurface freshwater flows to occur at surface pressures below 6.1 mbar (see Appendix A in Paper II for an example) because water vapor cannot escape quickly to the atmosphere.

#### 4.3. Flow

Once melted, the water will flow downhill from the bedrock unit and into the regolith. However, the diurnal skin depth in dry regolith is only 3–5 cm (Table 3). Therefore, the first percolation of water may turn to ice as it reaches these depths (see Appendix A in Paper II). Once volatiles enter regolith they will allow thermal energy to penetrate deeper into the subsurface, as ice- and water-rich regolith have skin depths similar to that of bedrock (Table 3). Also, surficial water (even in thin films) will reduce the surface albedo, allowing more solar insolation to be absorbed, further increasing surface and subsurface temperatures.

When RSL are active (dark and lengthening), they are stratified by depth. The shallowest portion of an RSL is the most unstable as it experiences the highest temperatures and is protected by the least amount of regolith. Therefore, any liquid water should evaporate away, which is consistent with the lack of detection of increased water signatures by CRISM (McEwen et al., 2011). However, RSL do darken the regolith. We suggest the darkening is caused by adsorbed water on a high surface area material, as laboratory experiments have shown is possible (Pommerol et al., 2009). Brushing from the Rock Abrasion Tool on the Mars Exploration Rovers and their rover tracks shows a thin layer of dust. This dust will have a grain size greater than or equal to the dust found in the atmosphere, which has been estimated to have a grain size of a few microns (Clancy et al., 1995; Pollack et al., 1995; Lemmon et al., 2004). Therefore, this surficial dust layer would have a large surface area capable of adsorbing water, which would darken its albedo. This adsorbed water is constantly replenished as the deeper layers provide water vapor as their liquid water evaporates.

Below the top few centimeters, liquid water would flow through the regolith during the daytime and freeze at night (e.g., Fig. S5). The thickness of this layer is uncertain, but it would increase with surface temperature, salt content of the liquid, and the thermal conductivity and decreasing gas diffusivity of the top few centimeters. Overall, we estimate this layer to be  $<15$  cm thick. This flowing liquid layer is then underlain by a low permeability layer, most likely ice due to the cold mean annual temperature.

In paper II, we model the amount of fresh water, hydraulic conductivity, evaporation rate, and vertical flow thickness of an individual 50 m RSL that flows for 60 sols. We find that 2–10  $m^3$  of  $H_2O$  per m of source headwall must be recharged each year under saturated flow, with a hydraulic conductivity equal to that of a well-sorted sand ( $\sim 3 \times 10^{-11} m^2$ ), an evaporation rate of 0.1  $mm h^{-1}$ , and a vertical flow thickness of several centimeters.

#### 4.4. Freezing and sublimation

SML RSL stop lengthening in late southern summer ( $L_s = 314^\circ \pm 12^\circ$ ) when near-maximum and mid-afternoon surface temperatures decrease below  $296 \pm 5$  and 273 K, respectively. We suggest that the SML RSL are frozen throughout the sol at this

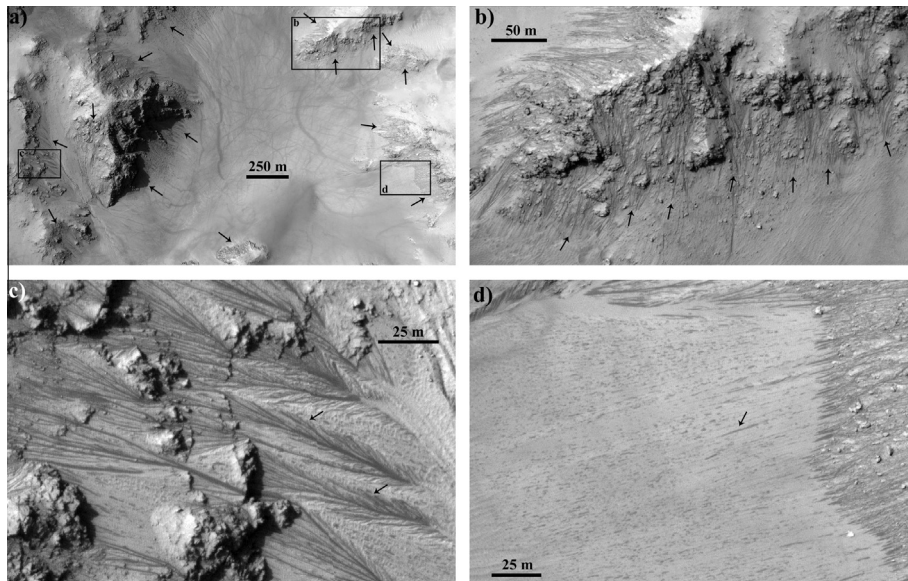


**Fig. 6.** (a) RSL emanate (shown with arrows) from every steep rocky slope just after the MY 28 dust storm in the central peak of Horowitz crater (32.04°S, 140.81°E). (b) From this mound RSL cascade downslope not only from equator-facing slopes, but also pole-facing slopes (arrows), which are only detected after the MY 28 dust storm. (c) A large density of flows that highlight the dendritic drainage patterns that are sourced from multiple bedrock elevations. Also note that the flows follow narrow channels that extend vertically, not laterally. The arrow highlights how some sources of water start from small ridges with no outcropping bedrock, which are only detected after the MY 28 dust storm. (d) RSL seem to stop in the middle of the scree slope, however discontinuous darkening is observed farther down the slope (see highlighting arrow), which are only detected after the MY 28 dust storm. This may suggest that some RSL continue underground and are wicked back up to the surface discontinuously. Images are cropped from the HiRISE image PSP\_005787\_1475 at MY 28 and  $L_s = 334.3^\circ$ .

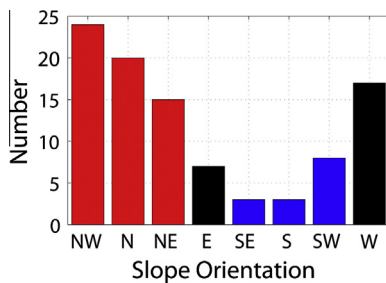


**Fig. 7.** Histogram of RSL slope facing direction for the SML RSL, where equator- and pole-facing slopes are shown in red and blue, respectively. Data can be found in the [supplemental spreadsheet](#). (For interpretation of the references to color in this figure legend, the reader is referred to the web version of this article.)

point. Without a liquid source, the frozen RSL begins to sublimate away. First, the pore ice of the RSL sublimates from the top down. This keeps the surface vapor pressure high enough to allow the persistence of adsorbed water, which allows static RSL to maintain an albedo darker than that of the surrounding terrain. This process continues into early southern fall ( $L_s = 16^\circ \pm 14^\circ$ ), or a duration of  $116 \pm 41$  sols.

The RSL then begin to fade, equaling or approaching the albedo of the surrounding material until late southern spring ( $L_s = 248^\circ \pm 11^\circ$ ) or  $228 \pm 21$  sols. This occurs when subsurface ice in the RSL can no longer maintain a high enough vapor pressure in the near-subsurface to maintain adsorbed water, which is necessary to provide albedo darkening. Therefore, subsurface adsorbed water and whatever ice still exists begin desorbing and sublimating, respectively. Eventually the ice that served as the aquitard for the RSL to flow upon begins to sublimate. However, its sublimation rate is greatly reduced due to the colder seasonal temperatures and amount of regolith overburden. Therefore, this ice does not fully sublimate and acts as a permeability barrier once RSL begin to flow again.

## 5. Discussion

In this section, we discuss how the MY 28 globe-encircling dust storm enhanced RSL, the long-term frequency of RSL, comparison of our flow mechanism to other RSL hypotheses, anomalous SML RSL sites, and lastly the astrobiological significance of our flow mechanism.

### 5.1. Post dust storm RSL enhancement

Abnormal RSL activity detected immediately after the MY 28 globe-encircling dust storm underscores the complexities and sensitivities of the formation process for RSL. Our observations of enhanced RSL flow distances as well as more sources, including non-bedrock sources, all suggest a warming of the subsurface (Figs. 4–6). While RSL are easier to detect due to a brightening of the surface due to dust fall (McEwen et al., 2011), observations at southwest Asimov Crater (Fig. 4) and the central peak of Lohse Crater (Fig. 5) demonstrate that this is not always the case.

The net energy gained and retained by the surface and subsurface during active RSL formation is a crucial metric in the discussion of how a dust storm might affect RSL, since it is this energy that largely determines whether, when, where, and how much water ice melts. A dust storm primarily alters the “normal” net energy situation at the surface by decreasing the energy received from sunlight (absorbed/scattered by the increased atmospheric dust) and increasing the downwelling infrared (IR) energy received (more emission from the extra-solar-heated dusty atmosphere) (e.g., Haberle and Jakosky, 1991). The net energy that the ground receives is not simple to define, however, as they necessarily exhibit complex functionality with respect to latitude, season, time-of-day, topographic slope, and poorly constrained variables (e.g., the size distribution of atmospheric dust as function of time and space).

Several lines of observational evidence exist that show/hint at what may happen to surface and subsurface temperatures during

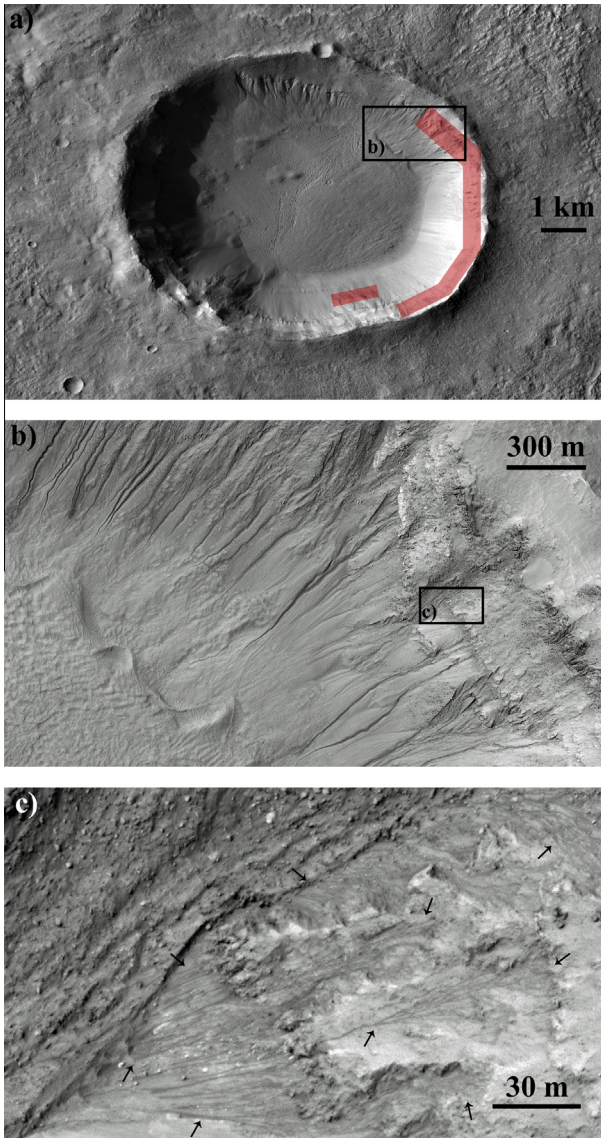


**Fig. 8.** (a) RSL Type IIa at the ~8 km diameter Corozal crater (43.32°S, 343.21°E) with detected RSL overlaid in red. Note the gullied walls and crater fill, which indicate this crater likely had volatile rich material in it. CTX image B04\_011390\_1409\_XN\_39S200. (b and c) Examples of RSL (arrows) in a pole-facing gully. HiRISE image ESP\_023218\_1410 at MY 30 and  $L_s = 325.7^\circ$ . (For interpretation of the references to color in this figure legend, the reader is referred to the web version of this article.)

a globe-encircling dust storm – however, all are less-than-ideal for quantifying what occurred in the southern mid-latitudes during the major MY 28 dust event. The influence of downwelling IR energy (which is poorly sensitive to slope azimuth) is potentially exemplified by a mound in the central peak of Horowitz crater in which RSL emanate from nearly every direction (Fig. 6b.). During the two large 1977 dust storms (at  $L_s \sim 205^\circ$  and  $279^\circ$ ), the Viking Lander 1 (VL1; at  $\sim 22.7^\circ$ N) observed that daily-maximum air temperatures (at  $\sim 1.6$  m above the ground) decreased by  $\sim 10$  K, while the daily-minimum temperatures increased by  $\sim 15$  K or more (Ryan and Henry, 1979). One might further assume that the VL1 near-surface air temperatures were significantly correlated with the ground surface temperature. This daytime (maximum) temperature depression is likely due to the dust-reduced daytime insolation loss being greater than the increased downwelling IR, and the nighttime (minimum) temperature increase is likely the result of the enhanced magnitude of the downwelling IR. However, it is

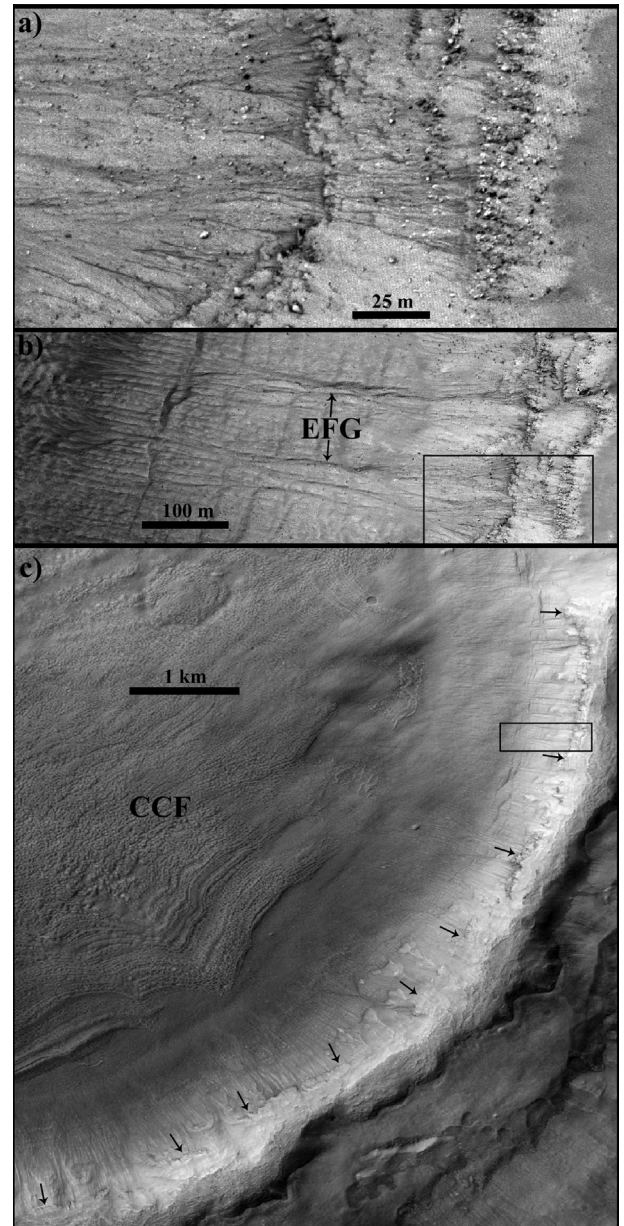


**Fig. 9.** (a) RSL originate out of multiple layers of bedrock and follow pre-existing topographic lows, presumably the drainage patterns of (b) equator-facing gullies (EFG). The arrows in (c) highlight the continuous bedrock outcrop where RSL are found continuously south of the northernmost arrow. This 11.5 km diameter unnamed crater has concentric crater fill (CCF) and is located on the eastern flanks of Hellas at  $39.6^\circ$ S,  $223.7^\circ$ E. Images are cropped from the HiRISE image PSP\_005934\_1400 at MY 28 and  $L_s = 340.5^\circ$ .

important to remember that these measurements were taken during autumn/winter in the northern hemisphere, when/where the maximum insolation is much reduced compared to that received by the SML RSL band ( $31\text{--}52^\circ$ S) at the same time. This general effect is also present in the TES spectrally-derived surface temperatures during the MY 25 (2001) globe-encircling dust storm, which began at  $L_s \sim 185^\circ$ . The TES surface temperature data also indicate that the effect varied significantly with latitude and with the maturity stage of the MY 25 dust storm. However, the MY 25 event had largely dissipated by  $L_s \sim 250\text{--}260^\circ$  in the southern mid-latitudes, while the MY 28 globe-encircling dust event began at  $L_s \sim 265^\circ$  and lasted throughout the typical SML RSL active season.

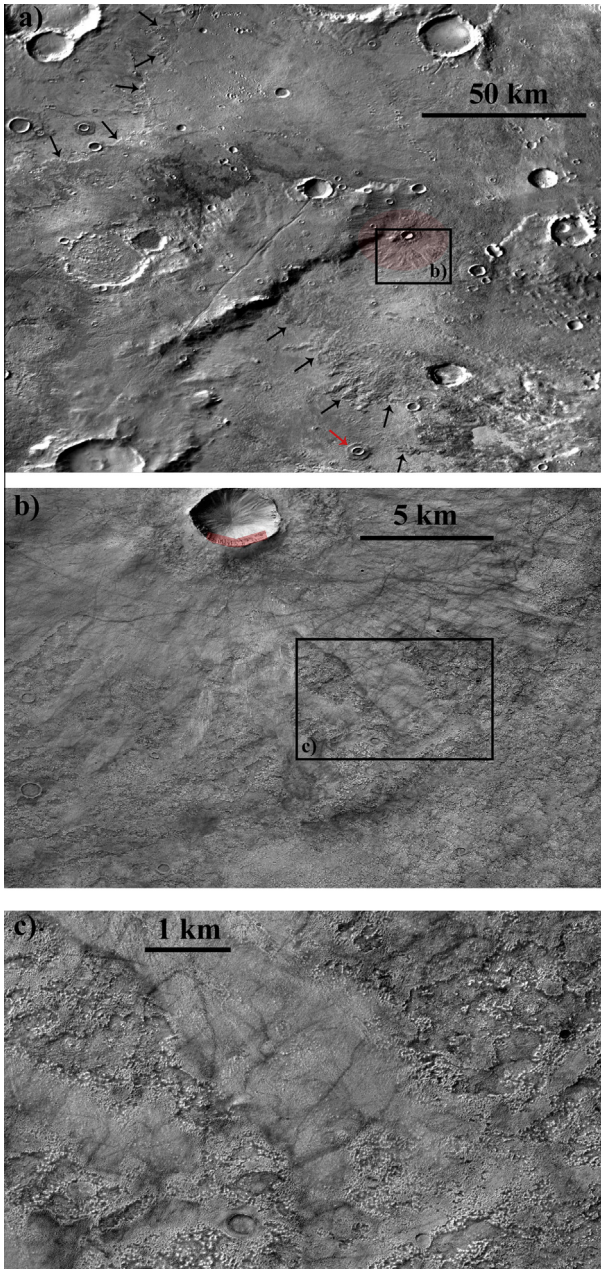


**Fig. 10.** (a) RSL type Ia at Raga crater (48.11°S, 242.44°E). This fresh crater seems to have impacted a volatile-rich unit that is sublimating. The front of this unit is highlighted by the black arrows and has left behind a pedestal crater (red arrow). Image is from the THEMIS Day IR 100 m Global Mosaic v 11.5. (b) The ejecta blanket, red overlay in (a), is smooth while the exposed volatile-rich unit is pitted. RSL are depicted by red overlay. Also, this crater appears to be young as it has no crater fill and poorly developed gullies. (c) This image shows how the ejecta blanket has protected this volatile-rich pitted unit. Images in (b) and (c) are from CTX image B11\_014011\_1317\_XN\_48S117W.

The net effect that this reduction of the diurnal temperature wave amplitude during a large dust storm has on subsurface temperatures is not clear-cut. Furthermore, for locations/seasons with abundant insolation, it is not even clear that the maximum surface temperature decreases during a major dust event. To help illuminate some plausible scenarios, a set of one-dimensional simulations of the atmosphere with an unslipped surface/subsurface for given latitudes and seasons were performed using a sophisticated radiative transfer code (see Appendix A for more details). The upper panel of Fig. 13a illustrates that ground surface

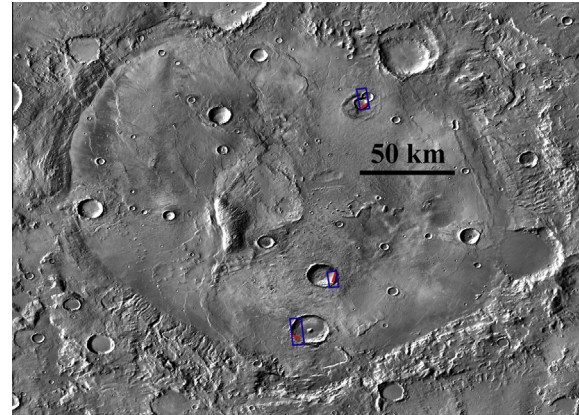


**Fig. 11.** Example of three RSL type IIa sites at Newton crater (40.5°S, 201.8°E) where the blue outlines are the boundaries of HiRISE images, and the red overlays highlighting where RSL were mapped. Image is from the THEMIS Day IR 100 m Global Mosaic v 11.5.

temperatures from a pair of one-dimensional simulations (see Appendix A for details) for 20°N (VL1-like) and  $L_s \sim 265^\circ$  (with and without a “dust storm”) behave similarly to the measured reduction in diurnal 1.6 m air temperature amplitude at VL1 during the major 1977 dust events. The upper panel of Fig. 13b is intended to exemplify surface temperature conditions at a southern mid-latitude RSL site during the MY 25 (2001) dust storm. It is similar to the VL1-like example, and correctly (qualitatively) reflects what was observed by TES. Note that the maximum diurnal subsurface temperatures (at  $\sim 5$  cm depth) of these two more similar cases (lower panels of Fig. 13a and b) do not show the significant cooling trend seen in the surface temperatures. The simulation results shown in Fig. 13c are meant to depict the conditions a few sols after the start of the MY 28 dust storm at a SML RSL site. In this case the surface temperatures do not significantly decrease, and peak subsurface temperature clearly increases. Here it appears that the significantly greater insolation (versus the other two cases) heats the dusty atmosphere enough to offset the loss of direct insolation to the surface (i.e., by significantly increasing the downwelling IR term). Additionally, other latitudes within the SML RSL zone exhibit similar thermal behavior at this season.

Thus, it appears entirely plausible that some places in the southern mid-latitudes may experience a net subsurface warming during a large dust storm, which in turn may lead to a significant enhancement of RSL activity there (e.g., Fig. 4). Furthermore, timing matters – SML RSL appear less likely to have been significantly affected by the globe-encircling dust storm of MY 25 than that of MY 28. Of course, these are only relatively simple 1-D simulations – many details such as topographic slopes and atmospheric transport of energy horizontally have yet to be addressed. More modeling and observational work is needed to better understand what actually happened to the RSL in MY 28.

Apparent non-bedrock sources, which were detected only after the MY 28 dust storm (Figs. 5 and 6), can be explained via two mechanisms. (1) Non-bedrock sources that emanate at the top of a ridge (Fig. 5) can be explained by ice-saturated regolith/bedrock covered by dry, low thermal conductivity regolith (Table 3). In summers without a large-scale dust event, temperatures at the regolith-ice interface do not exceed the melting point of ice. Only when subsurface temperatures are significantly raised, such as presumably during the MY 28 dust storm, can this reservoir of ice melt. (2) Non-bedrock sources that emanate at local divides (Fig. 6c) may be due to melting at the top of ice that acts as an aquitard. In both explanations, once the ice has melted and the top of the regolith becomes saturated by water, the regolith loses much

**Table 2**  
Classification of RSL types by geomorphology.

Type	Geomorphology	Example
Ia	Small (<15 km diameter) fresh crater	Fig. 10
Ib	Fossae	Fig. S3
IIa	Small (<20 km diameter) fresh crater within larger craters	Fig. 11
IIb	Central peaks	Figs. 6 and S4
IIIa	Steep slopes of large older craters	Fig. 12

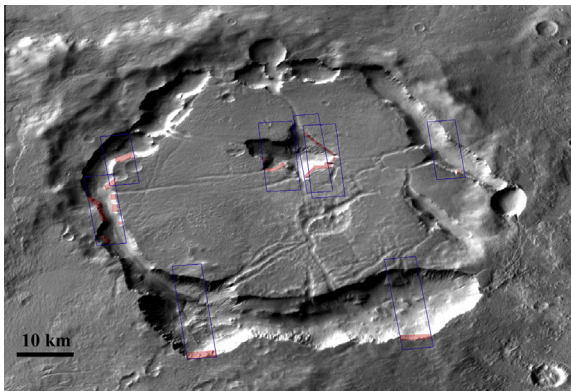


**Fig. 12.** Type III RSL are common throughout Asimov crater (47.0°S, 5.0°E) on any steep, outcropping bedrock slope that does not face directly poleward. Blue boxes indicate HiRISE images taken during a SML RSL season with dark albedo. Red boxes depict where RSL are observed. We estimate that with complete HiRISE imaging of the crater when RSL have dark albedo, RSL could be found along ~150 km of the steep slopes of Asimov crater. Image is from the THEMIS Day IR 100 m Global Mosaic v 11.5.

of its thermally-insulating properties, thereby allowing melting of additional non-bedrock sources. Overall, McEwen et al. (2011) argued that RSL lengths must be controlled by a limited volume of mobile material because RSL terminate on steep slopes. While true, we suggest that the limited volume is not due to lack of stored ice, but rather temperatures that are too cold to continue to melt subsurface ice.

## 5.2. Long-term frequency of RSL

The increased length and new non-bedrock sources of SML RSL after the MY 28 dust storm (Figs. 4–6), and the strong correlation of SML RSL lengthening with surface temperature (Fig. 3), strongly indicate that RSL flow is quite sensitive to surface temperature. Thus, SML RSL should not be observed where near-maximum and mid-afternoon surface temperatures fail to exceed a threshold temperature, possibly ~296 K and ~273 K, respectively. In order to explore the potential ramifications of this farther back in time, we computed and analyzed the mean insolation over the 100 sols (approximate length of RSL lengthening) each year that had the maximum daily insolation (for selected latitudes and an unsloped surface), based on martian orbital parameters for the past 5 million Earth-years (Laskar et al., 2004). Variations in insolation are not directly equated to surface temperature changes because of obfuscating atmosphere-coupled processes (e.g., the time- and spatially-varying atmospheric dust opacity and the seasonal emplacement and removal of surface CO<sub>2</sub>- and water-ice). Even so, it is probable that a significantly greater insolation will result in an increased surface temperature (and vice versa). In non-dust storm years, RSL are small, and we assume that the insolation

threshold to initiate SML RSL has to be near the current mean insolation value.

We find that the southern mid-latitudes of Mars last reached the current mean insolation values at ~100 ka (note that orbital parameter dates are given in Earth-years not Mars-years; Fig. 14a), and over the last 400 kyr at 45°S the insolation values are only greater than the current values ~4.7% of the time. Indeed, the current mean insolation value is at a maximum value in the southern hemisphere, presumably due to the current high eccentricity and the near-correspondence of the southern summer solstice ( $L_s$  270°) with the  $L_s$  of perihelion of 251°. At other mid-latitude pairs (e.g., 35°N/S and 55°N/S) the insolation trends are similar to that at 45°N/S (Figs. S6 and S7). Although the present-day 100-sol mean insolation (unsloped surface) values for 35–55°S are nearly identical (~260 W m<sup>-2</sup>), it is unclear whether this is a truly latitude-independent energetic threshold for SML RSL activation. Real-world factors that have not been accounted for in this insolation analysis include the significantly-sloped ground that RSL occur on and latitude- and time-dependent atmospheric dust loading. Items that further complicate this activation threshold interpretation include shallower subsurface ice deposits (if indeed the RSL are actually sourced from these) at higher latitudes and the variable length of daytime at each latitude.

Interestingly, the current mean insolation value at 45°N during an assumed northern RSL season is near a minimum, and has been higher for the majority (90.5%) of the last 400 ka. This is consistent with the observations that only two northern mid-latitude RSL sites have been detected poleward of 18°N, compared with 32 SML RSL sites. Therefore, the strong present-day prevalence for SML RSL may occur because the insolation during the active RSL season (and thus surface/subsurface temperatures) is greater there than it has been in the last 100 ka.

Furthermore, based on the assumptions above, over the last 5 Ma or 3 Ma, SML RSL would occur only ~15.5% or 8.2% of the time, respectively (Fig. 14b). Between 5 and 3 Ma, mean insolation was frequently more than 10% higher than current values (Fig. 14b). Given enough metastable ice, these periods may have led to large-magnitude RSL that may have formed the equator-facing fine gullies and channels.

## 5.3. Comparison to other hypotheses

McEwen et al. (2011) suggested a much longer duration for SML RSL activity of 240 sols ( $L_s = 240$ – $20$ ). This longer duration leads to a colder peak surface temperature cutoff of ~250 K, which in combination with the greater stability of brine led McEwen et al. (2011) to suggest brine flow in the shallow subsurface as a possible RSL SML mechanism. This duration also led Chevrier and Rivera-Valentin (2012) to propose a possible mechanism to reduce evaporation rates to allow brine flow within 20 cm of the surface with a liquid freezing temperature of ~223 K. We also believe that the thermal conductivity on a darkened regolith would drastically increase due to the interconnected thin water film paths (e.g., Piqueux and Christensen, 2009). Therefore, the thermal properties of the ground would be more similar to wet regolith than to the dry regolith modeled by Chevrier and Rivera-Valentin (2012) and allow thermal energy to penetrate much deeper into the subsurface (Fig. S5 and Paper II). Furthermore, by breaking the dark albedo category into lengthening and static categories we found that the vast majority of SML RSL only lengthen for  $104 \pm 38$  sols ( $L_s = 248^\circ \pm 114^\circ$  to  $314^\circ \pm 12^\circ$ ) when average near-maximum TES-derived surface temperatures are  $298 \pm 5$  K and mid-afternoon surface temperatures are >273 K. This shorter duration brackets surface and subsurface temperatures that are greater than the freezing point of fresh water for many hours during the day (Fig. S5). Therefore, brines are not necessary for RSL-like flow.

**Table 3**  
Differences in thermal properties of regolith and bedrock. Thermal inertia varies from 180 to 342 J m<sup>-2</sup> s<sup>-1/2</sup> K<sup>-1</sup> (McEwen et al., 2011) with an average value of 257 J m<sup>-2</sup> s<sup>-1/2</sup> K<sup>-1</sup>.

	Thermal conductivity (W m <sup>-1</sup> K <sup>-1</sup> )	Volumetric heat capacity × 10 <sup>-6</sup> (J K <sup>-1</sup> m <sup>-3</sup> )	Thermal inertia (J m <sup>-2</sup> s <sup>-1/2</sup> K <sup>-1</sup> )	Diurnal skin depth (m)	Annual skin depth (m)	Annual phase lag (°)
Dry regolith <sup>a</sup>	0.045	1.381	249.3	0.030	0.78	73.0z
In situ dry regolith <sup>b</sup>	0.085	1.050	298.7	0.048	1.2	46.3z
Water-saturated regolith	2.5	3.050	2761	0.15	3.9	14.6z
Bedrock <sup>a</sup>	2.5	2.176	2333	0.18	4.7	12.3z

<sup>a</sup> Sizemore and Mellon (2006).

<sup>b</sup> Zent et al. (2010).

Subsurface brine flow is much easier to accomplish thermally than fresh water flow, but both are plausible. The brine flow model has two weaknesses: (1) the high concentration of salt needed to significantly reduce water activity and (2) salt recharge. Chevrier and Rivera-Valentin (2012) argued that salt would be dissolved from the regolith. Indeed, the martian regolith is salty, but the Mars Phoenix lander only found 10 mM of dissolved salt with ~0.4–0.6 wt% ClO<sub>4</sub> within the regolith (Hecht et al., 2009). This concentration is considered brackish and is two orders of magnitude lower than the needed eutectic composition. Secondly, if the RSL are composed of brine, their high salt content would be transported downslope as the RSL lengthened. The water would then evaporate/sublimate away leaving salt in the subsurface downslope of the source. This repetitive or constant transport of salt would relatively rapidly flush all easily available salts from the source regions. Without any salt recharge mechanism, the salt would then have to be dissolved from increasingly distant surrounding bedrock or regolith. However, a near eutectic concentration of salt requires 10s of wt% salt. No subsidence or headwall erosion has yet been observed (Kite, 2013). Future studies are needed to monitor for this erosion and determine the salt content of the outcropping bedrock units from which the RSL emanate. Currently, there is no evidence that the bedrock or regolith possesses such significant amounts of salt and no evidence of salt has been detected via orbital spectroscopy at RSL termini. However, some salts (chlorides) are virtually undetectable by spectroscopy. Furthermore, these salts may all be in the subsurface, completely undetectable via orbital measurements. Another probable scenario for briny flows could be from a shallow briny aquifer. However, it is thermally difficult to maintain a briny aquifer in such proximity to the surface, unless it had a significant freezing point depression (e.g., -60 °C). If it has a significant freezing point depression then why do RSL only lengthen once the afternoon temperatures exceed 273 K? Furthermore, it is difficult to imagine an aquifer feeding the RSL found on the steep slopes on the central peak of craters (e.g., Fig. 6b).

Levy et al., 2011 suggested that Antarctic water tracks (WT), which are only active during the warmest months, may be morphologically or genetically similar to RSL. These WT are classified as “salt superhighways” (Levy et al., 2011) and provide salts to the most saline natural body of water on Earth, Don Juan Pond (Dickson et al., 2013). The salt and liquid water are both ultimately sourced from snow (Levy et al., 2011). The majority of WT sampled by Levy et al. (2011) are brackish, with only the most concentrated WT sample considered saline. Significant quantities of cations were not reported, making the freezing depression of this sample uncertain. However, assuming a maximum 0.8 M concentration (8 wt%) of CaCl<sub>2</sub> the freezing depression should be less than 4 K. While CaCl<sub>2</sub> has a eutectic temperature of 223 K, >80% of the water in the most concentrated WT sample would have to freeze out before reaching the eutectic composition. This ice would clog the pores, significantly reduce the hydraulic conductivity, increase the viscosity by 32%, and significantly reduce the volume of water left to flow. Therefore, even with salt recharge from snow, these “salt

superhighways” do not transport brine concentrations of salt that would significantly reduce the freezing point of water.

Overall, our hypothesis suggests that subsurface freshwater flows create the SML RSL. As this freshwater flows it would dissolve any salt it comes in contact with in the bedrock or regolith. Therefore, the salt concentration of RSL flows may be similar to that of the fresh-to-saline Antarctic WT concentrations.

#### 5.4. Discussion of anomalous RSL sites

We analyzed 249 HiRISE images at 32 confirmed and candidate southern mid-latitude RSL sites over four martian years and found anomalous formation at six of these sites (Fig. 2). The confirmed RSL site in southwest Asimov crater (47.6°S, 4.6°E) does not lengthen between MY 28 L<sub>s</sub> 343.3° and MY 29 L<sub>s</sub> 11.3°, but then anomalously a single long RSL lengthens in the subsequent image (MY 29 L<sub>s</sub> 19.1°). Subsurface temperatures during this period are likely too cold for pure water flows and rarely reach above 250 K, thus making brine flow challenging as well. More data is needed to see if this typically occurs at this site or if this was somehow related to the globe-encircling dust storm earlier in the season. We consider this to be an outlier, as data from the other RSL sites stop lengthening at L<sub>s</sub> = 314° ± 12°.

The second and third anomalous RSL sites occur in unnamed craters (40.3°S, 319.7°E and 34.1°S, 134.5°E) at candidate RSL sites. Both of these locations clearly show RSL that emanate from non-bedrock sources during certain years. Anomalously, RSL are not detected every year. We believe that these two sites again demonstrate how sensitive to temperature RSL are, and that without bedrock (i.e., high thermal conductivity) the high subsurface temperatures needed to melt ice may not occur every year.

The fourth anomalous RSL site occurs in an unnamed crater (38.1°S, 224°E) at a confirmed RSL site. Here, the RSL activity started after L<sub>s</sub> 279° in MY 31 and before L<sub>s</sub> 281.3° in MY 30. The MY 31 observations suggest that these RSL begin later than the majority of the SML RSL (L<sub>s</sub> 248° ± 11°). The bedrock source units of these RSL face southeast, and this is the only location where SML RSL have a bright band outlining them. We currently consider this an outlier, as the late start of these RSL was only captured in MY 31. If it occurs again, enhanced thermal modeling will be needed to determine whether the southeast-facing orientation of the bedrock there could delay the lengthening phase of these RSL. Another hypothesis is that this is a unique type of RSL, potentially recognizable by their bright perimeter band.

The last two anomalous sites occur at the central peak of Hale crater (35.7°S, 323.5°E and 35.6°S, 323.6°E). These two candidate RSL sites are very close together, with HiRISE images of these two sites overlapping in places. HiRISE has only acquired two images of the more northern site in MY 29; these show long RSL at L<sub>s</sub> 222.6°, but no additional lengthening in the subsequent image at L<sub>s</sub> 243.3°. The other site shows long RSL in its first HiRISE image at MY 31 L<sub>s</sub> 256.8°. This site's RSL continue to lengthen until L<sub>s</sub> 287.7° and then anomalously, they partially fade in the next HiRISE

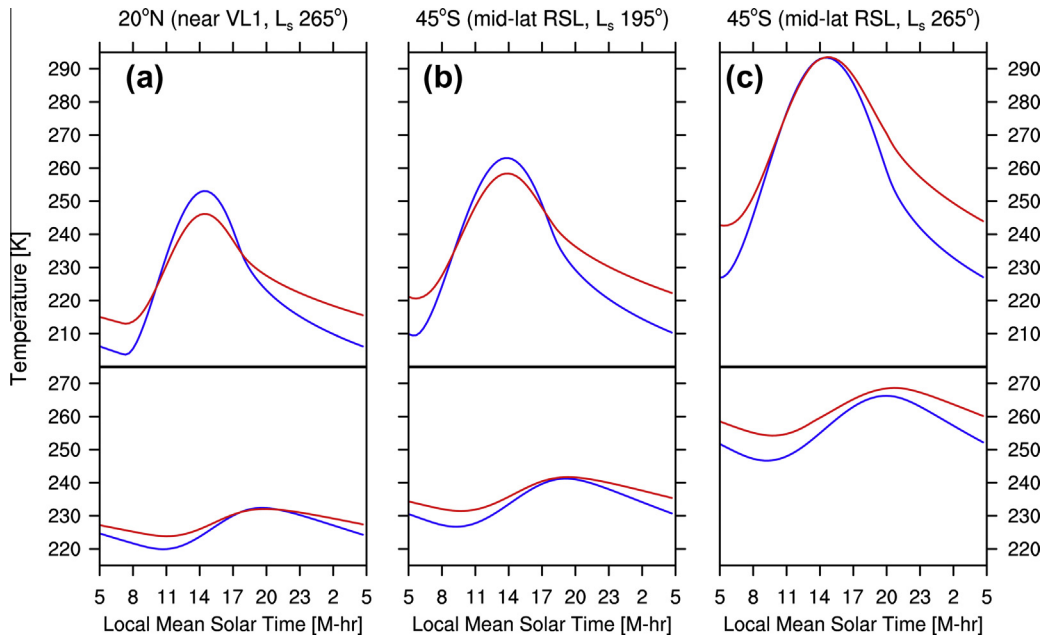


**Fig. 13.** Results from 1-D modeling (see Appendix A for more details), showing ground surface temperature (upper panels) and subsurface temperature at  $\sim 5$  cm (lower panels) versus time-of-day for “normal” conditions (blue curves) and “dust storm” conditions (red curves; 3rd full sol after dust storm initiation). (a)  $20^\circ\text{N}$ ,  $L_s \sim 265^\circ$ , intended to emulate solstitial dust storm conditions at the VL1 site, (b)  $45^\circ\text{S}$ ,  $L_s \sim 195^\circ$ , meant to reflect conditions at a SML RSL site during the MY 25 (2001) dust storm, (c)  $45^\circ\text{S}$ ,  $L_s \sim 265^\circ$ , mimicking conditions at a southern mid-latitude RSL site during the MY 28 (2007) dust storm. Note that the 5 cm subsurface value does not reach 273 K for this flat site. Equatorial-facing slopes should be warmer, plus RSL typically emanate from bedrock that has a much higher thermal conductivity than modeled here in this general example. (For interpretation of the references to color in this figure legend, the reader is referred to the web version of this article.)

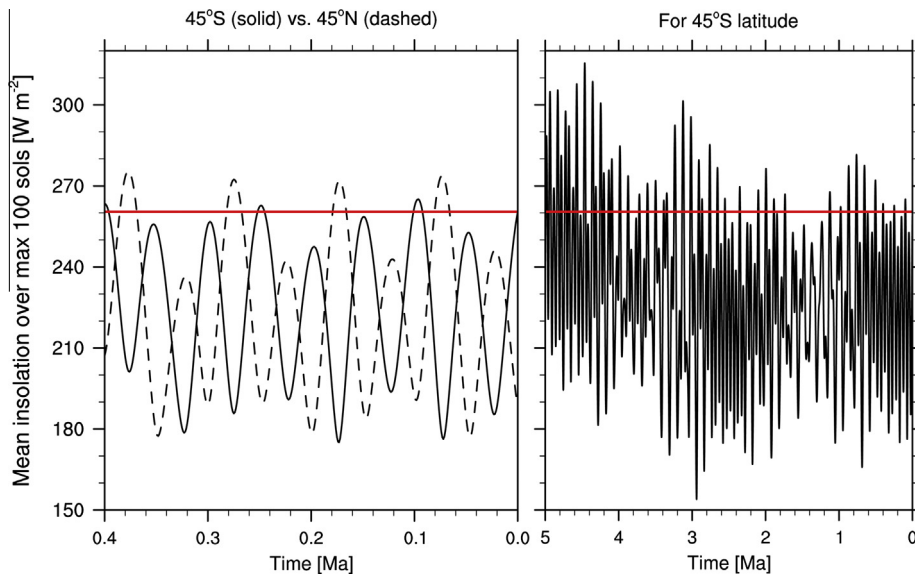


**Fig. 14.** Mean insolation for a level surface over the 100 sols each year that had the maximum daily average insolation at specified latitudes based on the last (a) 400 ka and (b) 5 Ma of orbital parameters (Laskar et al., 2004). The horizontal line represents the current value of this mean insolation quantity at  $45^\circ\text{S}$  and illustrates that only in 4.7%, 8.2%, and 15.5% of the last 0.4, 3, and 5 Ma have the mean insolation quantity been greater than current values, respectively. The last time the southern hemisphere had a mean insolation quantity this high was  $\sim 100$  ka. The mean insolation quantity for  $45^\circ\text{N}$  has had a greater magnitude 90.5% of the time, to 400 ka. This suggests that any northern mid-latitude RSL formation would have been more likely 75 ka.

image at  $L_s 326.9^\circ$ . It appears that a second burst of RSL activity then occurs, as RSL begin to re-lengthen in the subsequent two HiRISE images taken at  $L_s 329.7^\circ$  and  $341.9^\circ$ . More HiRISE data is needed to monitor whether the anomalous behaviors (early lengthening SML RSL, early stopping and fading, and re-lengthening) occur yearly here. The anomalous periods at Hale crater before and after the typical SML RSL activity interval interestingly

correspond to two large (regional) southern mid-latitude dust events that occur in each year that lacks a globe-encircling dust storm (i.e., MY 24, MY 26, MY 29, MY 30, MY 31; Kass et al., 2013). The first typically initiates between  $L_s 210^\circ$  and  $240^\circ$  and lasts for  $15\text{--}40^\circ$  of  $L_s$ , and the latter begins within  $L_s 305\text{--}320^\circ$  and lasts for  $3\text{--}15^\circ$  of  $L_s$ . Further data analysis is needed to determine whether these dust events significantly affected Hale crater,

and modeling is required to bolster the case that a regional dust storm at  $L_s \sim 220^\circ$  and  $\sim 330^\circ$  at this latitude can increase subsurface temperatures and influence RSL behavior.

### 5.5. Astrobiological significance

Fresh liquid water that recurs yearly of astrobiological significance as it is clearly advantageous for extant life. Organic matter in Antarctic water track soils is 5–10 times higher than in the surrounding dry soils (Levy and Fountain, 2011). However, we suggest that yearly SML RSL flows only occur under favorable conditions with dry intervals lasting for  $\sim 100$  kyr. Consequently, radiation-resistant microbes may only need to be reanimated every  $\sim 100$  kyr if sequestered at depths  $>1$  m (Dartnell et al., 2007). This presents a narrow interval between the minimum depth for microbe survival and the maximum melting depth of cold-trapped ice. Nonetheless, because organisms or detritus would likely be flushed out by flow, RSL tracks on accessible lower slopes may be some of the best locations on Mars to search for extant life.

## 6. Conclusions

Our analysis suggests that SML RSL lengthen for  $104 \pm 38$  sols (Fig. 2), while near-maximum and mid-afternoon surface temperatures are  $298 \pm 5$  K and  $>273$  K, respectively (Fig. 3), which allow subsurface temperature to obtain temperatures  $>273.16$  K for a few hours each sol (Fig. S5). We also found that the MY 28 dust storm greatly enhanced RSL density, length, and apparent non-bedrock sources indicating that flows are quite sensitive to putative increased subsurface temperatures associated with the occurrence of the dust storm (Figs. 4–6). One-dimensional modeling results (Fig. 13) further demonstrated that the southern mid-latitude subsurface conditions during the MY 28 dust storm may have actually been warmer than in other years. RSL appear to be linked to the equator-facing fine gullies and channels, as they appear to emanate from similar bedrock units (Figs. 8 and 9).

While salts are ubiquitous on Mars (e.g., Wang et al., 2006; Hecht et al., 2009) and would significantly increase the stability of water, liquid water covered by a low gas diffusivity regolith also retards water evaporation regardless of salt content. Our observations show that near-maximum and mid-afternoon temperatures are  $>273$  K (Fig. 3), and therefore the water flowing in the RSL does not need to be briny. This eliminates the need to replenish salt reservoirs every year. Therefore, we suggest that the majority of the SML RSL are caused by shallow freshwater subsurface flows. However, the mechanism that recharges this water remains unknown.

Furthermore, we suggest that RSL occurrence corresponds with epochs and latitudes that have sustained periods (e.g., tens to  $>100$  sols) of daily mean insolation each Mars-year that have substantially greater magnitudes than the longer-term average (i.e., over tens to hundreds of thousands of Earth-years) for that latitude. Currently, the southern mid-latitudes are receiving more intense insolation for part of each year than they have for the last  $\sim 100$  ka (Fig. 14a). Meanwhile, the northern mid-latitudes are near a  $\sim 50$  kyr minimum in their maximum yearly insolation intensity, receiving  $\sim 27\%$  less mean insolation than the southern mid-latitudes. These findings, along with the increased activity post dust storm, lead us to suggest that RSL are intermittent and have only recently started in the southern mid-latitudes; any northern mid-latitude RSL were much more likely to flow at  $\sim 75$  ka than today. Future HiRISE, THEMIS, and MCS observations along with enhanced atmospheric, thermal, and hydrological modeling will further test and refine this hypothesis.

## Acknowledgments

This work was aided by discussion with Mark Bullock, Scot Rafkin, and Mikki Osterloo. This work was supported by the NASA Mars Fundamental Research Program, Grants NNX12AH99G (R.E.G., K.P.H.) and NNX12AH95G (D.E.S.). We would like to thank Alfred McEwen and Colin Dundas for providing exceptionally detailed and constructive reviews.

## Appendix A

The one-dimensional (1-D) simulation results described in Section 5.1 were performed with the Mars Regional Atmospheric Modeling System (MRAMS; e.g., Michaels and Rafkin 2008; Rafkin et al., 2001). A two-stream radiative transfer code was used that employs a correlated-k method for gaseous absorption, with dust absorption and multiple aerosol scattering based on the optical properties of spherical particles of Hawaiian palagonite (Michaels and Rafkin, 2008). The atmospheric domain used 69 vertical layers (increasing geometrically in thickness with altitude), with the lowest layer midpoint  $\sim 5$  m above ground and the model top at  $\sim 65$  km. The multi-layer surface/subsurface thermal model used in this work has 47 layers, and starting with a top layer 1 mm thick, layer thicknesses increase geometrically with a stretch ratio of 1.12 (lowest layer midpoint is  $\sim 1.6$  m below the surface). A dry thermal conductivity of  $0.085 \text{ W m}^{-1} \text{ K}^{-1}$  was used in all runs, along with a volumetric heat capacity of  $1.0665 \times 10^6 \text{ J K}^{-1} \text{ m}^{-3}$ , resulting in an effective thermal inertia of  $\sim 300$  (SI units).

Each run was 15 sols in duration, and the simulations were done in pairs for ease in comparison/contrast: a “normal” scenario, and a “dust storm” case. Horizontal advection, turbulent diffusion, water–ice and  $\text{CO}_2$ –ice microphysics were turned off. Vertical turbulent diffusion and advection for non-aerosol variables was turned on. All simulations had a radiatively-active background dust loading set to “normal” year dust opacities from TES (Smith 2004) as a function of latitude and season. The “dust storm” cases were identical to the “normal” cases until 6 sols had elapsed, at which time a foreground dust optical depth of 1.0 (at a wavelength of  $\sim 9 \mu\text{m}$ , referenced to 6.1 hPa) was imposed, well-mixed throughout the lower  $\sim 40$  km of the atmosphere. All dust in these runs was not subject to advection, gravitational sedimentation, or turbulent diffusion. The initial state of the atmosphere and subsurface was taken from a prior 3-D mesoscale simulation at  $45^\circ\text{S}$ ,  $L_s \sim 265^\circ$  – the 6-sol spin-up period was employed to allow a significant amount of thermal equilibration to the local season/location to occur.

## Appendix B. Supplementary material

Supplementary data associated with this article can be found, in the online version, at <http://dx.doi.org/10.1016/j.icarus.2014.01.017>.

## References

- Altheide, T.S., Chevrier, V., Nicholson, C., Denson, J., 2009. Experimental investigation of the stability and evaporation of sulfate and chloride brines on Mars. *Earth Planet. Sci. Lett.* 282, 69–78. <http://dx.doi.org/10.1016/j.epsl.2009.03.002>.
- Bryson, K.L., Chevrier, V., Sears, D.W.G., Ulrich, R., 2008. Stability of ice on Mars and the water vapor diurnal cycle: Experimental study of the sublimation of ice through a fine-grained basaltic regolith. *Icarus* 196, 446–458. <http://dx.doi.org/10.1016/j.icarus.2008.02.011>.
- Chevrier, V.F., Rivera-Valentin, E.G., 2012. Formation of recurring slope lineae by liquid brines on present-day Mars. *Geophys. Res. Lett.* 39, L21202. <http://dx.doi.org/10.1029/2012GL054119>.

- Chevrier, V. et al., 2007. The sublimation rate of ice under simulated Mars conditions and the effect of layers of mock regolith JSC Mars-1. *Geophys. Res. Lett.* 34, L02203. <http://dx.doi.org/10.1029/2006GL028401>.
- Chevrier, V., Ostrowski, D.R., Sears, D.W.G., 2008. Experimental study of the sublimation of ice through an unconsolidated clay layer: Implications for the stability of ice on Mars and the possible diurnal variations in atmospheric water. *Icarus* 196, 459–476.
- Christensen, P.R., 2003. 2001 Mars Odyssey, Thermal Emission Imaging System (THEMIS), Data Processing User's Guide, [http://starbase.jpl.nasa.gov/ody-mthm-2-visiredr-packtest-v1.0/ody\\_0000/document/process.pdf](http://starbase.jpl.nasa.gov/ody-mthm-2-visiredr-packtest-v1.0/ody_0000/document/process.pdf), 37 pgs.
- Christensen, P.R., 2006. Mars Global Surveyor, Thermal Emission Spectrometer, Data Processing User's Guide. <http://tes.asu.edu/mgst/document/process.pdf>, 38 pgs.
- Christensen, P.R. et al., 2001. Mars Global Surveyor Thermal Emission Spectrometer experiment: Investigation description and surface science results. *J. Geophys. Res.* 106 (E10), 23,823–23,871.
- Christensen, P.R. et al., 2004. The Thermal Emission Imaging System (THEMIS) for the Mars 2001 Odyssey Mission. *Space Sci. Rev.* 110, 85–130.
- Clancy, R.T., Lee, S.W., Gladstone, G.R., McMillan, W., Roush, T., 1995. A new model for Mars atmospheric dust based upon analysis of ultraviolet through infrared observations from Mariner 9, Viking, and Phobos. *J. Geophys. Res.* 100, 5251–5263.
- Clancy, R.T. et al., 2000. An intercomparison of ground-based millimeter, MGS TES, and Viking atmospheric temperature measurements: Seasonal and interannual variability of temperatures and dust loading in the global Mars atmosphere. *J. Geophys. Res.* 105 (E4), 9553–9571.
- Dartnell, L.R., Desorgher, L., Ward, J.M., Coates, A.J., 2007. Modelling the surface and subsurface martian radiation environment: Implications for astrobology. *Geophys. Res. Lett.* 34, L02207. <http://dx.doi.org/10.1029/2006GL027494>.
- Dickson, J.L., Head, J.W., Levy, J.S., Marchant, D.R., 2013. Don Juan Pond, Antarctica: Seasonal near-surface CaCl<sub>2</sub>-rich brine transport feeding the most saline lake on Earth and implications for Mars. *Sci. Rep.* 3. <http://dx.doi.org/10.1038/srep01166>.
- Dundas, C.M. et al., 2012. Seasonal activity and morphological changes in martian gullies. *Icarus* 220, 124–143.
- Gough, R.V., Chevrier, V.F., Baustian, K.J., Wise, M.E., Tolbert, M.A., 2011. Laboratory studies of perchlorate phase transitions: Support for metastable aqueous perchlorate solutions on Mars. *Earth Planet. Sci. Lett.* 312, 371–377.
- Grimm, R.E., Harrison, K.P., Stillman, D.E., 2014. Water budgets of martian recurring slope lineae. *Icarus*, 27 pages (in press).
- Haberle, R.M., Jakosky, B.M., 1991. Atmospheric effects on the remote determination of thermal inertia of Mars. *Icarus* 90, 187–204.
- Hayne, P.O. et al., 2012. Carbon dioxide snow clouds on Mars: South polar winter observations by the Mars Climate Sounder. *J. Geophys. Res.* 117, E08014. <http://dx.doi.org/10.1029/2011JE004040>.
- Hecht, M.H. et al., 2009. Detection of perchlorate and the soluble chemistry of martian soil at the Phoenix Lander Site. *Science* 325, 64–67.
- Kass, et al., 2013. Inter-annual similarities during the martian dusty season. In: 45th Meeting of the Division of Planetary Sciences, October 6–11, Denver, CO.
- Kite, E.S., 2013. Mass balance constraints on the sustainability of Mars' recurrent slope lineae (RSL): Should RSL be an astrobiology priority? The Present-Day Habitability of Mars, 4–6 February, Los Angeles, CA, 74-Kite\_Habitability\_2013.pdf.
- Kreslavsky, M.A., Head, J.W., 2000. Kilometer-scale roughness of Mars: Results from MOLA data analysis. *J. Geophys. Res.* 105 (E11), 26695–26712.
- Kreslavsky, M.A., Head, J.W., 2002. Mars: nature and evolution of young latitude-dependent water-ice-rich mantle. *Geophys. Res. Lett.* 29 (15). <http://dx.doi.org/10.1029/2002GL015392>.
- Laskar, J., Gastineau, M., Joutel, F., Robutel, P., Levrard, B., Correia, A., 2004. Long term evolution and chaotic diffusion of the insolation quantities of Mars. *Icarus* 170, 343–364.
- Lemmon, M.T. et al., 2004. Atmospheric imaging results from the Mars Exploration Rovers: Spirit and opportunity. *Science* 306, 1753–1756. <http://dx.doi.org/10.1126/science.1104474>.
- Levy, J., 2012. Hydrological characteristics of recurrent slope lineae on Mars: Evidence for liquid flow through regolith and comparisons with Antarctic terrestrial analogs. *Icarus* 219, 1–4. <http://dx.doi.org/10.1016/j.icarus.2012.02.016>.
- Levy, J.S., Fountain, A.G., 2011. Antarctic dry valley water tracks and permafrost wet patches: Ecosystem and astrobiological implications of water exchange between salts, soils, and the atmosphere in a Mars-analog cold desert. In: Fifth International Mars Polar Conference, Fairbanks, AK. Abstract #6054.
- Levy, J. et al., 2011. Water tracks and permafrost in Taylor Valley, Antarctica: Extensive and shallow groundwater connectivity in a cold desert ecosystem. *Geol. Soc. Am. Bull.* 123, 2295–2311. <http://dx.doi.org/10.1130/B30436.1>.
- Malin, M.C., Edgett, K.S., 2000. Evidence for recent groundwater seepage and surface runoff on Mars. *Science* 288, 2330–2335. <http://dx.doi.org/10.1126/science.288.5475.2330>.
- Malin, M.C. et al., 2007. Context Camera Investigation on board the Mars Reconnaissance Orbiter. *J. Geophys. Res.* 112, E05S04. <http://dx.doi.org/10.1029/2006JE002808>.
- McCleese, D.J. et al., 2007. Mars Climate Sounder: An investigation of thermal and water vapor structure, dust and condensate distributions in the atmosphere, and energy balance of the polar regions. *J. Geophys. Res.* 112, E05S06. <http://dx.doi.org/10.1029/2006JE002790>.
- McEwen, A.S. et al., 2007. Mars Reconnaissance Orbiter's High Resolution Imaging Science Experiment (HiRISE). *J. Geophys. Res.* 112, E05S02. <http://dx.doi.org/10.1029/2005JE002605>.
- McEwen, A.S. et al., 2011. Seasonal flows on warm martian slopes. *Science* 333, 740–743. <http://dx.doi.org/10.1126/science.1204816>.
- McEwen, A.S. et al., 2013. Recurring slope lineae (RSL): Flow of briny water on present-day Mars? In: The Present-Day Habitability of Mars, 4–6 February, Los Angeles, CA, 36-RSL-Mars-Habitability-2013.pdf.
- Mellon, M.T., Phillips, R.J., 2001. Recent gullies on Mars and the source of liquid water. *J. Geophys. Res.* 106, 23165–23180.
- Michaels, T.I., Rafkin, S.C.R., 2008. Meteorological predictions for candidate 2007 Phoenix Mars Lander sites using the Mars Regional Atmospheric Modeling System (MRAMS). *J. Geophys. Res.* 113, E00A07. <http://dx.doi.org/10.1029/2007JE003013>.
- Mustard, J.F., Cooper, C.D., Rifkin, M.K., 2001. Evidence for recent climate change on Mars from the identification of youthful near-surface ground ice. *Nature* 412, 411–414.
- Ojha, L. et al., 2013. Spectral constraints on the nature and formation mechanism of recurring slope lineae. In: The Present-Day Habitability of Mars, 4–6 February, Los Angeles, CA, 55-Ojha\_Habitability\_2013\_UCLA\_V4.pdf.
- Piqueux, S., Christensen, P.R., 2009. A model of thermal conductivity for planetary soils: 2. Theory for cemented soils. *J. Geophys. Res.* 114, E09006. <http://dx.doi.org/10.1029/2008JE003309>.
- Pollack, J.B., Ockert-Bell, M.E., Shepard, M.K., 1995. Viking Lander image analysis of martian atmospheric dust. *J. Geophys. Res.* 100, 5235–5250.
- Pommerol, A., Schmitt, B., Beck, P., Brissaud, O., 2009. Water sorption on martian regolith analogs: Thermodynamics and near-infrared reflectance spectroscopy. *Icarus* 204, 114–136. <http://dx.doi.org/10.1016/j.icarus.2009.06.013>.
- Rafkin, S.C.R., Haberle, R.M., Michaels, T.I., 2001. The Mars Regional Atmospheric Modeling System: Model description and selected simulations. *Icarus* 151, 228–256. <http://dx.doi.org/10.1006/icar.2011.6605>.
- Ryan, J.A., Henry, R.M., 1979. Mars atmospheric phenomena during major dust storms, as measured at surface. *J. Geophys. Res.* 84 (B6), 2821–2829. <http://dx.doi.org/10.1029/JGRE0000840000B6002821000001>.
- Sizemore, H.G., Mellon, M.T., 2006. Effects of soil heterogeneity on martian ground-ice stability and orbital estimates of ice table depth. *Icarus* 185, 358–369.
- Smith, M.D., 2004. Interannual variability in TES atmospheric observations of Mars during 1999–2003. *Icarus* 167, 148–165. <http://dx.doi.org/10.1016/j.icarus.2003.09.010>.
- Tillman, J.E., Johnson, N.C., Guttrop, P., Percival, D.B., 1993. The martian annual atmospheric pressure cycle: Years without great dust storms. *J. Geophys. Res.* 84, 10,963–10,971 (special edition).
- Wang, A. et al., 2006. Sulfate deposition in subsurface regolith in Gusev crater, Mars. *J. Geophys. Res.* 111, E02S17. <http://dx.doi.org/10.1029/2005JE002513>.
- Wang, A., Lu, Y., Chou, L., 2013. Recurring slope lineae (RSL) and subsurface chloride hydrates on Mars. In: Lunar Planet. Sci., 44 (The Woodlands, March 18–22, 2606.pdf).
- Zent, A.P. et al., 2010. Initial results from the thermal and electrical conductivity probe (TECP) on Phoenix. *J. Geophys. Res.* 115, E00E14. <http://dx.doi.org/10.1029/2009JE003420>.